LETTERS

Preseismic velocity changes observed from active source monitoring at the Parkfield SAFOD drill site

Fenglin Niu[1], Paul G. Silver[2], Thomas M. Daley[3], Xin Cheng[1] & Ernest L. Majer[3]

Measuring stress changes within seismically active fault zones has been a long-sought goal of seismology. One approach is to exploit the stress dependence of seismic wave velocity, and we have investigated this in an active source cross-well experiment at the San Andreas Fault Observatory at Depth (SAFOD) drill site. Here we show that stress changes are indeed measurable using this technique. Over a two-month period, we observed an excellent anti-correlation between changes in the time required for a shear wave to travel through the rock along a fixed pathway (a few microseconds) and variations in barometric pressure. We also observed two large excursions in the travel-time data that are coincident with two earthquakes that are among those predicted to produce the largest coseismic stress changes at SAFOD. The two excursions started approximately 10 and 2 hours before the events, respectively, suggesting that they may be related to pre-rupture stress induced changes in crack properties, as observed in early laboratory studies[1,2].

It is well known from laboratory experiments that seismic velocities vary with the level of applied stress[3–5]. Such dependence is attributed to the opening and closing of microcracks due to changes in the stress normal to the crack surface[6–8]. In principle, this dependence constitutes a stress meter, provided that the induced velocity changes can be measured precisely and continuously. Indeed, there were several attempts in the 1970s to accomplish this goal using either explosive or non-explosive surface sources[9–11]. The source repeatability and the precision in travel-time measurement appeared to be the main challenges in making conclusive observations.

With the availability of highly repeatable sources, modern data acquisition systems and advanced computational capability, Yamamura *et al.*[12] showed compelling evidence that seismic velocity along a baseline in a vault near the coast of Miura Bay, Japan, responds regularly to tidal stress changes. Silver *et al.*[13] found an unambiguous dependence of seismic velocity on barometric pressure from a series of cross-well experiments at two test sites in California. The stress sensitivity depends primarily on crack density and has a strong nonlinear dependence on confining pressure. Consequently, crack density is expected to decrease rapidly with depth, as should stress sensitivity. It is thus unclear whether the stress-induced velocity variations observed at shallow depths[12,13] are still detectable at seismogenic depth.

To explore stress sensitivity at seismogenic depth, we have conducted an experiment at Parkfield, California, where adjacent deep wells, namely the SAFOD pilot and main holes (Fig. 1), are available. Accurately located seismicity, together with the availability of high-quality geophysical data in the Parkfield region, make it one of the best areas to detect temporal changes related to the earthquake cycle. A specially designed 18-element piezoelectric source and a three-component accelerometer were deployed inside the pilot and main holes, respectively, at ~1 km depth (see Methods). The experiment was conducted for ~2 months: the first period was 29 October to 28

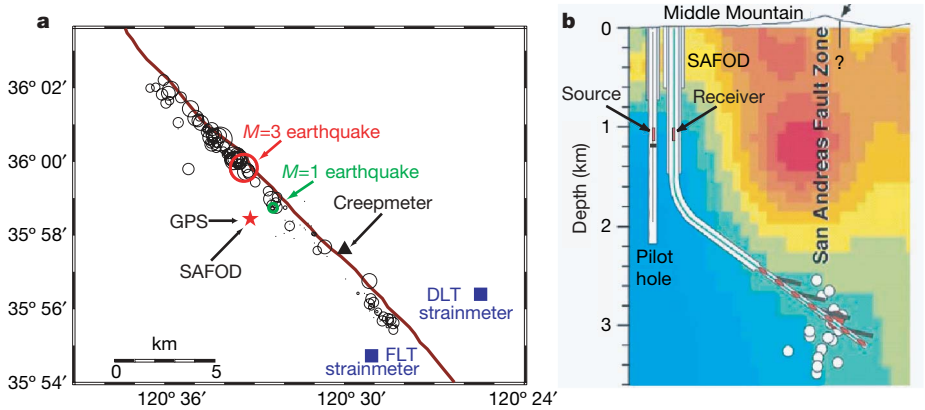

Figure 1 | Map of the experiment site. a, Circles show earthquakes that occurred during the experiment period. The $M = 3$ and $M = 1$ events are shown as red and green circles, respectively. Star indicates the Parkfield SAFOD drill site, where the experiment was conducted. Triangle, location of the Middle Mountain creepmeter; squares, locations of the Donalee (DLT) and Frolich (FLT) Gladwin borehole tensor strainmeters. **b**, A vertical section (schematic) of the SAFOD main and pilot holes. Red vertical lines indicate the source and receiver locations. Background image is electrical resistivity[18] with blue (red) corresponding to relatively high (low) resistivity. White circles show the seismicity, red dashes indicate the SAFOD instrumentation, and black short lines represent sub-horizontal holes drilled off the main hole. The profile at the top of the panel is the surface topography with the arrow indicating the surface exposure of the fault.

[1]Department of Earth Science, MS-126, Rice University, 6100 Main Street, Houston, Texas 77005, USA. [2]Department of Terrestrial Magnetism, Carnegie Institution of Washington, 5241 Broad Branch Road, NW, Washington DC 20015, USA. [3]Earth Sciences Division, Lawrence Berkeley National Laboratory, 1 Cyclotron Road, Berkeley, California 94720, USA.

November 2005, and the second was 11 December 2005 to 10 January 2006. We fired a pulse with a width of 1 ms four times per second and recorded 200-ms-long data with a sampling rate of 48,000 Hz. The waveforms were automatically stacked in groups of 100 shots, resulting in one record (Fig. 2) acquired every 27 s (two additional seconds were needed in storing the data).

To enhance the signal-to-noise ratio (SNR) of the data, we further stacked the raw seismograms in sets of 100. This stacking procedure reduced the data to one stack every 45 min. The 45-min stacked records were then processed with a bandpass filter of 1–5 kHz before the travel-time analysis. We used a cross-correlation-based method to estimate the delay time, which permits subsample precision (see Methods). No smoothing or filtering was applied to the measured delay time series. The error in delay time measurement was estimated to be $\sim 1.1 \times 10^{-7}$ s, based on SNR analysis (see Methods), and this estimate was confirmed by comparing measurements from consecutive recordings. As the nominal travel time of the shear-wave (S-wave) coda along the baseline is about 10 ms, the detectable threshold of velocity perturbation is $\sim 1.1 \times 10^{-5}$, or 11 p.p.m.

We measured the delay times of the S wave and the S wave plus its coda up to 20 ms with respect to a fixed reference trace for each period (Fig. 3). The measurements show daily cycles that are well correlated with the temperature record (Fig. 3). Silver *et al.*[13] found that this temperature sensitivity originates from the electronics of the recording system rather than from changes in the subsurface velocity field. We excluded the measurements of the first few days to allow the source and sensor to be stabilized at their locations. We also removed the linear trend from the data as was done by Silver *et al.*[13]. In general, the delay times of the coda are about twice as large as those of the S wave, suggesting that they are caused by a change in the velocity of the bulk media, as the coda travels for a longer time in the media and thus is expected to accumulate a larger travel-time anomaly. The delay time closely follows the barometric pressure changes for the first period (Fig. 3a).

After removing the temperature effect from the measured delay time variations (Fig. 3a), we obtained a delay time change of ~ 3.0 μs in the first period. The corresponding velocity perturbation is about 3×10^{-4}, about an order of magnitude higher than the detectable threshold. During the same time period, the change in barometric pressure is ~ 1.3 kPa. We used a linear regression to estimate the stress sensitivity of the velocity and obtained a value of 2.4×10^{-7} Pa^{-1}. We also calculated the predicted solid Earth tides at the site in the same period and found that the tidal stress varies within 240 Pa, nearly an order of magnitude smaller than changes in barometric pressure. Thus the travel-time changes induced by tidal stress are of the order of 10^{-7} s, close to the measurement error and thus are predicted to be undetectable.

The negative correlation between travel time and barometric stress can be further seen in the delay time data through to the end of the ninth day of the second period. After this time the relationship starts to break down, and we observe instead two prominent excursions in the delay time data that are not seen in the barometric pressure record. It is also confirmed that the two excursions were not caused by precipitation or instrumentation. The amplitudes of the two excursions are ~ 5.5 μs and ~ 1.5 μs, respectively, over the nominal ~ 10 ms coda travel time. Using our measured stress sensitivity of 2.4×10^{-7} Pa^{-1}, the corresponding stress changes are 2.3 kPa and 625 Pa for the first and second peak, respectively.

In order to evaluate the possibility of a tectonic cause for the excursions, we examined the seismicity around the SAFOD site occurring in the experiment period (Fig. 4a). The first peak appears to correspond to the largest earthquake occurring in this period (date, 24 December 2005; time, 10:10:57.21 (h:min:s UT); location, 35.9970° N, 120.5565° W; depth, 3.88 km; magnitude 3.00, hereafter the $M = 3$ event), while the second peak corresponds to the second closest (1.5 km) event to the experiment site (29 December 2005, 01:32:50.87 UT, 35.9788° N, 120.5397° W, depth 1.82 km, magnitude 0.98, hereafter the $M = 1$ event). The closest event is about 1.3 km away from our site, but its size is only $M = 0.34$ and thus should not have a large effect at the site.

We calculated the predicted static stress change at SAFOD associated with these two earthquakes. The near-field static displacement at a location $\mathbf{r}$ with respect to the earthquake is proportional to $M_o r^{-2}$, where M_o is the seismic moment[14]. The spatial derivative of

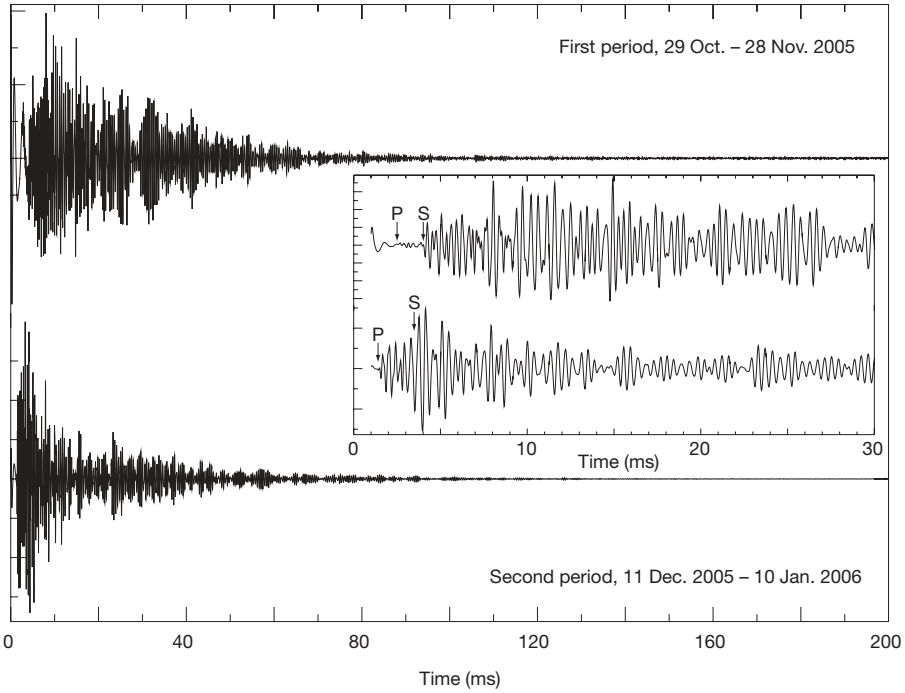

Figure 2 | An example of the raw seismograms obtained from a horizontal component in the two periods. Both are filtered with a band pass filter of 1–5 kHz. Inset shows the first 30 ms of the waveforms. P and S indicate the compressional and shear wave arrivals.

displacement, strain, thus should be $\propto M_o r^{-3}$. The static stress change at **r** is $\Delta\sigma = a\frac{\mu L^2 D}{r^3} = a\frac{\mu(D/L)}{(r/L)^3} = a\frac{\Delta\sigma_o}{\hat{r}^3}$, where $\Delta\sigma_o$ is the average static stress change along the fault, $\hat{r}$ is the characteristic distance measured in fault lengths (L), D is slip on the fault, μ is the shear modulus, and a is a scaling constant equal to $1/(6\pi)$ (ref. 14). If we assume a static stress change in the range of 3 to 10 MPa (refs 15, 16), then the static coseismic stress change at the SAFOD site is estimated to be ~250–833 Pa for the $M = 3$ event, which is a few times lower than the total stress change (2.3 kPa) calculated from the amount of delay time during the first excursion. The predicted static stress changes at the SAFOD site calculated from the entire local seismicity catalogue are shown in Fig. 4b. Here we used all the events that occurred within 10 km of the site and made a time series of the coseismic stress changes. The $M = 3$ earthquake obviously has the largest effect at the experiment site. The second largest peak around day 20 corresponds to a relatively deep event (22 November 2005, 03:38:02.13 UT, 36.0100 −120.5692, depth 5.07 km, $M = 2.6$), which is not observed in the delay time data. The third peak corresponds to the $M = 1$ event. It is not clear to us why the larger $M = 2.6$ event is not observed while the smaller $M = 1$ event shows clearly in the delay time data. But we noticed that data collected in the second period had a better SNR than those of the first period. The associated stress change of the $M = 2.6$ event thus might be below the resolution of the first-month data.

Coseismic change was also observed in other geodetic data. We found a step-function change from the borehole fibre-optic strainmeter data at SAFOD (Fig. 4a inset) as well as from the surface creepmeter data at Middle Mountain (Fig. 4b). The static strain change observed at SAFOD is $\sim(20\text{–}25) \times 10^{-9}$, corresponding to

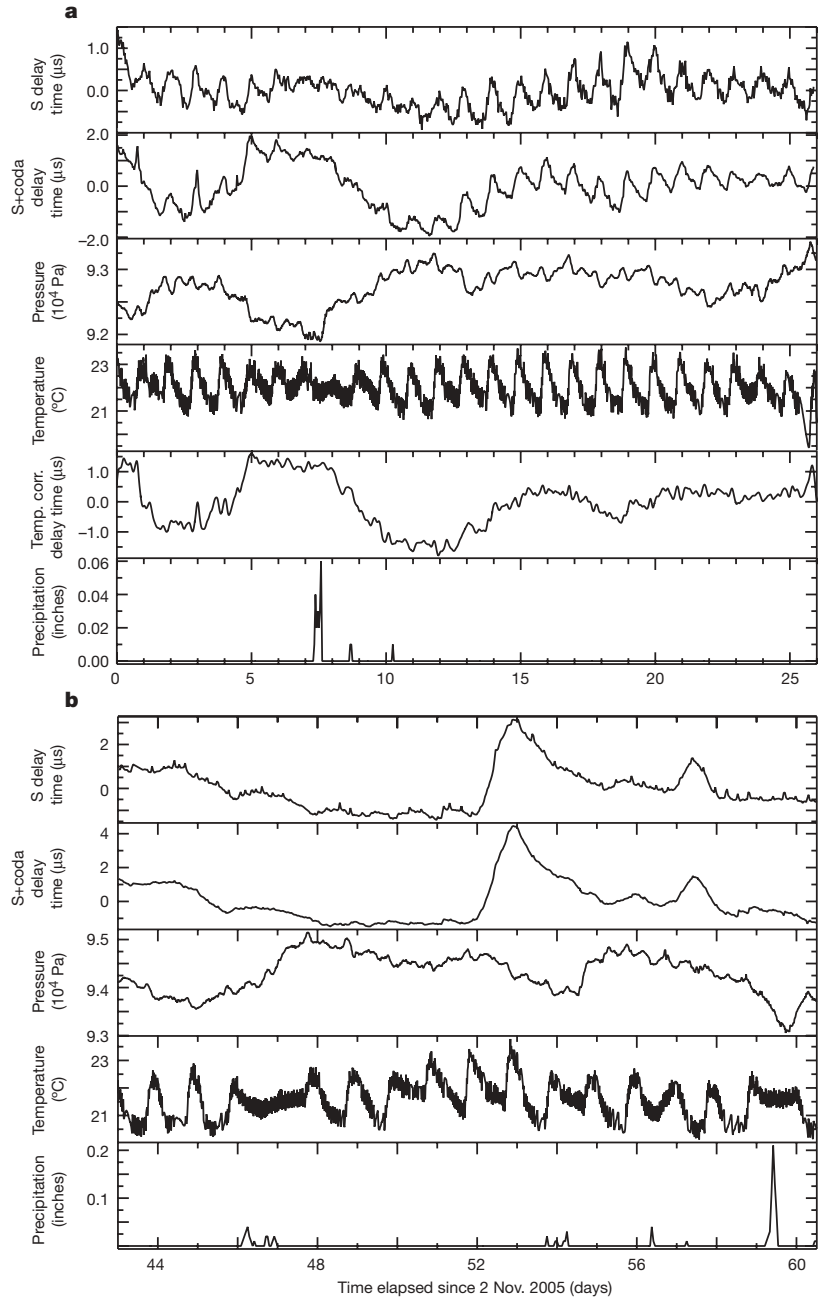

Figure 3 | Estimated delay times for the two periods. **a**, First period; **b**, second period. In each panel, the top two traces are delay times estimated from time windows that contain respectively the S-wave arrival and the S-wave arrival plus the coda; the third trace is barometric pressure; the fourth trace is temperature; and the bottom trace is precipitation. In **a**, the second to last trace is a temperature corrected version of the second trace. Elapsed time is calculated from 2 November 2005, 00:00:00 UT.

a coseismic stress change of ~600–750 Pa, which is of the same order of magnitude as our estimate. On the other hand, there were no obvious changes in the SAFOD GPS, or the FLT and DLT strainmeter records (Fig 4b). The lack of an observable coseismic signal at these sites is, however, predicted by the theoretical amplitude.

The coseismic offset recorded by the SAFOD strainmeter is not obviously present in the delay time data measured either from the manually stacked 45-min-per-sample data or from the delay times calculated from the 27-s-per-sample raw data. The derivative of the delay time series (dotted line in Fig. 4c), however, does reveal that the largest offset of the entire two-month observing period occurred ~30 s after the $M = 3$ earthquake. This suggests that there was a small coseismic change in the delay time data. The lack of a stronger coseismic signal in the delay time data may imply that the velocity changes we observed here are mainly the result of a poroelastic[17] rather than an elastic response to abrupt stress changes.

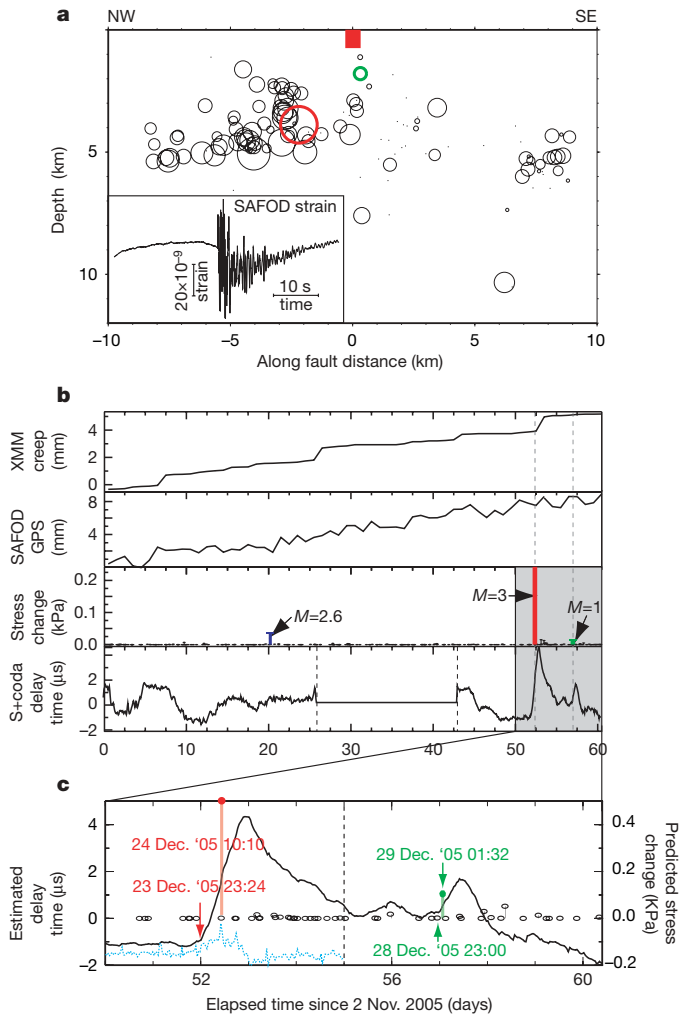

Figure 4 | A comparison of delay time variations with local seismicity and other deformation measurements. **a**, Depth distribution of earthquakes that occurred in the experimental period. Red square, the SAFOD experiment site; red and green circles, the $M = 3$ and $M = 1$ earthquake, respectively. Inset, the SAFOD strainmeter record, which shows a step-function coseismic strain change. The low frequency content of the strainmeter data is severely contaminated by surface temperature variations, and is consequently not suitable for analysis. **b**, Top to bottom: creep measurement at Middle Mountain (XMM); GPS measurement of fault-parallel motion at the SAFOD site; calculated static coseismic stress changes at the SAFOD experiment site for all of the earthquakes; and delay times estimated from the S wave plus its coda for comparison. Dashed lines indicate the time when the $M = 3$ and $M = 1$ earthquakes occurred. Note that the amplitude of the stress change of the $M = 3$ event (~0.5 kPa) is saturated in this plot. **c**, Predicted coseismic stress changes at SAFOD for earthquakes occurring between 22 December 2005 (day 50) and 1 January 2006 (day 60) indicated by shading in **b** are shown with the delay time estimation. Stress changes from the local seismicity between days 55 and 60 are amplified by a factor of 10. The two filled circles show the stress change of the $M = 3$ (red) and $M = 1$ (green) event, respectively. The vertical lines indicate the occurrence times of the $M = 3$ and the $M = 1$ event, and the red and green (upward) arrows show the onset times of the two excursions. Blue dotted line is the derivative of the delay time series. Notice that the largest change occurred about ~30 s after the $M = 3$ earthquake.

The two travel-time excursions appear to possess significant preseismic components. The first excursion was observed to start at 23:34 UT on 23 December 2005, while the $M = 3$ earthquake occurred at ~10.6 h later, at 10:10 UT on 24 December 2005 (Fig. 4c). The excursion reached a maximum right after the earthquake, peaking at 21:21 UT on 24 December 2005. The excursion thus has a clear preseismic component besides the coseismic/postseismic changes. The preseismic and coseismic/postseismic components account for ~46% and ~54% of the total change, respectively. This is also true for the second excursion. Its onset is around 22:59 UT on 28 December 2005, about 2.5 h before the occurrence of the $M = 1$ earthquake (01:32 UT on 29 December, Fig. 4c).

With the available geodetic instrumentation, it was impossible to further evaluate the preseismic component. The most direct test would have been with the SAFOD borehole strainmeter data. Unfortunately, the low frequency component is severely contaminated by surface temperature variations and is unusable for periods longer than a few minutes, and is thus not useful in confirming the two low-frequency excursions (M. Zumberge, personal communication). All other instrumentation is either too far away or not sufficiently sensitive to observe even the coseismic offset. Historically, there has been an absence of preseismic signals in geodetic observations, such as a borehole strainmeter. We suggest that this may be the result of two differences between such instruments and our 'stress meter'. First, our basic measurement is not strain, but rather a stress-induced change in the effective elastic constants of a poroelastic medium, mediated by variations in crack properties and fluid flow. These changes may register only weakly on a strainmeter, a GPS, or a creepmeter. Second, a conventional strainmeter measures local change in the volume immediately surrounding the instrument while our measurements reflect stress/strain changes occurring over a volume sampled by the coda waves that could be orders of magnitude larger.

We put forward the hypothesis that there is a change in effective elastic moduli before rupture, such as a sudden increase in microcrack density, which is a phenomenon related to dilatancy and observed in many laboratory studies[1,2]. As such, further continuous seismic monitoring might provide an effective tool for understanding the stress changes that accompany and perhaps precede seismic activity.

METHODS SUMMARY

We used a specially built piezoelectric source and a Geode recorder (Geometrics) to generate and record seismic waves travelling along a ~10 m baseline near the San Andreas fault at ~1 km depth. A cosine fitting method was used to estimate the S-wave travel time to subsample precision.

Full Methods and any associated references are available in the online version of the paper at www.nature.com/nature.

Received 22 October 2007; accepted 12 May 2008.

1. Brace, W. F., Paulding, B. W. & Scholz, C. H. Dilatancy in the fracture of crystalline rocks. *J. Geophys. Res.* **71**, 3939–3953 (1966).
2. Scholz, C. H. Microfracturing and the inelastic deformation of rock I: Compression. *J. Geophys. Res.* **73**, 1417–1432 (1968).
3. Birch, F. The velocity of compressional waves in rocks to 10 kilobars, part 1. *J. Geophys. Res.* **65**, 1083–1102 (1960).
4. Birch, F. The velocity of compressional waves in rocks to 10 kilobars, part 2. *J. Geophys. Res.* **66**, 2199–2224 (1961).
5. Nur, A. & Simmons, G. The effect of saturation on velocity in low porosity rocks. *Earth Planet. Sci. Lett.* **7**, 183–193 (1969).
6. Walsh, J. B. The effect of cracks on the compressibility of rock. *J. Geophys. Res.* **70**, 381–389 (1965).

7. Nur, A. Effects of stress on velocity anisotropy in rocks with cracks. *J. Geophys. Res.* **76,** 2022–2034 (1971).
8. O'Connell, R. J. & Budiansky, B. Seismic velocities in dry and saturated cracked solids. *J. Geophys. Res.* **79,** 5412–5426 (1974).
9. De Fazio, T. L., Aki, K. & Alba, J. Solid earth tide and observed change in the in situ seismic velocity. *J. Geophys. Res.* **78,** 1319–1322 (1973).
10. Reasenberg, P. & Aki, K. A precise, continuous measurement of seismic velocity for monitoring in situ stress. *J. Geophys. Res.* **79,** 399–406 (1974).
11. Leary, P. C., Malin, P. E., Phinny, R. A., Brocher, T. & Voncolln, R. Systematic monitoring of millisecond traveltime variations near Palmdale, California. *J. Geophys. Res.* **84,** 659–666 (1979).
12. Yamamura, K. *et al.* Long-term observation of in situ seismic velocity and attenuation. *J. Geophys. Res.* **108,** doi:10.1029/2002JB002005 (2003).
13. Silver, P. G., Daley, T. M., Niu, F. & Majer, E. L. Active source monitoring of cross-well seismic traveltime for stress-induced changes. *Bull. Seismol. Soc. Am.* **97,** 281–293 (2007).
14. Aki, K. & Richards, P. G. *Quantitative Seismology* (Freeman, New York, 1980).
15. Abercrombie, R. E. Earthquake source scaling relationships from −1 to 5 M_L using seismograms recorded at 2.5-km depth. *J. Geophys. Res.* **100,** 24015–24036 (1995).
16. Rubin, A. M. & Gillard, D. Aftershock asymmetry/rupture directivity among central San Andreas fault microearthquakes. *J. Geophys. Res.* **105,** 19095–19109 (2000).
17. Segall, P., Jonsson, S. & Agustsson, K. When is the strain in the meter the same as the strain in the rock? *Geophys. Res. Lett.* **30,** doi:10.1029/2003GL017995 (2003).
18. Unsworth, M., Bedrosian, P., Eisel, M., Egbert, G. & Siripunvaraporn, W. Along strike variations in the electrical structure of the San Andreas Fault at Parkfield, California. *Geophys. Res. Lett.* **27,** 3021–3024 (2000).

Acknowledgements We thank the NSF funded SAFOD programme and those involved in providing the experiment site, R. Trautz for supplying the barometric pressure logger, M. Zumberge for providing the SAFOD strainmeter data, and D. Lippert and R. Haught for helping with field work. This work was supported by the NSF, Rice University, the Carnegie Institution of Washington, and Lawrence Berkeley National Laboratory of the US Department of Energy under contract DE-AC02-05CH11231.

Author Information Reprints and permissions information is available at www.nature.com/reprints. Correspondence and requests for materials should be addressed to F.N. (niu@rice.edu).

METHODS

Data acquisition system. Our acquisition was conducted with a combination of commercial and specially built equipment. The latter are the piezoelectric source and the high voltage amplifier used to power it. The source includes 18 cylindrical rings of piezoelectric ceramic (lead zirconate titanate) epoxied together and wired for positive and negative voltage on the inner and outer surfaces. The source was fluid coupled to the well casing. A three-component accelerometer was clamped to the well casing to provide coupling and reduce relative motions between the source and receiver. We used a commercial recording system, a 'Geode' manufactured by Geometrics, which has a 24 bit analogue-to-digital converter. An air conditioner and heater were used to maintain the recording system electronics within a temperature range of about $\pm 1\,^{\circ}\mathrm{C}$.

Triggering was used in our data recording system. The digitizer continually samples the data, and receives a trigger that will generally be between two digitized samples. Including a section of pre-trigger data, the time series is interpolated and resampled, so that the new time series begins at the time of the trigger. This start time is not exact, and, at a sampling rate of 48,000 s^{-1}, this time is computed to the nearest twentieth of a sample (Geometrics engineering, personal communication). Thus there is a delay time measurement error that will be at most a fortieth of a sample (half-way between samples), and the average error will be an eightieth of a sample, assuming that the errors are uniformly distributed. This corresponds to an average error of 260 ns per trigger. The error in the stacked data decreases by a factor of $N^{1/2}$, assuming the errors are uncorrelated. For $N = 100$, we obtain a timing error of 26 ns.

Optimum experimental design. As shown by Silver *et al.*[13], there is an optimum distance between the source and receiver that minimizes the detectable threshold of subtle velocity changes:

$$N = Q/\pi \tag{1}$$

Here N is the number of wavelengths between the source and receiver and Q is the quality factor. At the SAFOD site, Q is around 200, which gives $N = 64$. If we assume the S-wave velocity to be 2.8 m ms^{-1}, then the wavelength of the signal with a dominant frequency of 2 kHz is about 1.4 m, so the optimum distance is ~90 m. As it was necessary to perform the experiment in the available boreholes, our cross-hole distance was limited to 10 m, which while not optimal still provided us with a good SNR.

Subsample delay time estimate (DTE). In this study, we employed a cosine fitting method to estimate subsample delay time in the time domain[19,20]. Given the largest sample of the correlation function, cc(0), and its two neighbours cc(−1) and cc(1), the estimated subsample shift is given by following expression:

$$\tau = \alpha / \arctan\left(\frac{\mathrm{cc}(-1) - \mathrm{cc}(1)}{2\mathrm{cc}(0)\sin\alpha}\right) \tag{2}$$

where:

$$\alpha = \arccos\left(\frac{\mathrm{cc}(-1) + \mathrm{cc}(1)}{2\mathrm{cc}(0)}\right) \tag{3}$$

Error estimation. *Silver et al.*[13] derived a low bound of the error in delay time measurements:

$$\sigma_{\mathrm{DTE}} \geq \frac{1}{2\pi f_0 \mathrm{SNR}} \tag{4}$$

Here f_0 is the dominant frequency of the source pulse, and SNR is the signal-to-noise ratio. Equation (4) indicates that SNR is the only parameter that controls the precision in our delay time estimation when the digitizing error is much less than the background noise in this regime. The precision is not controlled by the sampling rate of the digitizer so it is possible to obtain subsample-interval measurements of the delay time. The dominant frequency of our data is 2 kHz and the SNR is around 700 for the 45-min stacked data, resulting in a best achievable precision of $\sim 1.1 \times 10^{-7}$ s, or 110 ns in the DTE.

We also measured delay time between each two consecutive samples, which follows a gaussian distribution with a standard deviation of ~80 ns and ~50 ns for the first and second recording period, respectively. In general they are comparable to or even better than the theoretical low bound in equation (4). Since there is contribution from the actual stress-induced velocity perturbations in the measurement, our actual precision can be better than the measured standard deviations. Thus the lower bound appears to be larger than the true DTE error. One possible explanation is that the SNR is significantly underestimated, as the noise is estimated from a time window before the first arrival, which actually contains a considerable amount of non-random electronic noise known as cross-talk, and non-random 'wrap-around' noise from the previous shot.

The precision discussed here does not include other systematic non-random noise, such as changes in the source pulses, errors in trigger timing and digitizer's clock. Such systematic errors could lead to a long-term trend in DTE. To estimate these effects, we also recorded the source pulse waveform in addition to the data. We employed the same method to measure the variation in the source pulse width. Changes in the source pulse width are between ±20 ns. This indicates that our source pulse generator and recording system were very stable in the two periods and timing error in the digitizer clock was also very small.

19. Cespedes, I., Huang, Y., Ophir, J. & Spratt, S. Methods for estimation of subsample time delays of digitized echo signals. *Ultrason. Imaging* **17**, 142–171 (1995).
20. De Jong, P. G. M., Arts, T., Hoeks, A. P. G. & Reneman, R. S. Determination of tissue motion velocity by correlation interpolation of pulsed ultrasonic echo signals. *Ultrason. Imaging* **12**, 84–98 (1990).